Received: 1 February 2019 | Accepted: 6 December 2019

DOI: 10.1002/hyp.13700

SCIENTIFIC BRIEFING

HP TODAY WILEY

Modifying the Jackson index to quantify the relationship between geology, landscape structure, and water transit time in steep wet headwaters

Christopher P. Gabrielli[1] | Jeff J. McDonnell[1,2]

[1]Global Institute for Water Security, University of Saskatchewan, Saskatoon, Saskatchewan, Canada

[2]School of Geography, Earth & Environmental Sciences, University of Birmingham, Birmingham, UK

Correspondence
Christopher P. Gabrielli, Global Institute for Water Security, University of Saskatchewan, 11 Innovation Boulevard, Saskatoon, SK S7N 3H5, Canada.
Email: chris.gabrielli@usask.ca

Funding information
AGU Horton Research Grant; Canadian Network for Research and Innovation in Machining Technology, Natural Sciences and Engineering Research Council of Canada; National Science Foundation, Grant/Award Number: DEB-1440409

Abstract

The relationship between stream water mean transit time (MTT), catchment geology, and landscape structure is still poorly characterized. Here, we present a new simple index that builds on the Jackson, Bitew, and Du (2014) index that focuses specifically on permeability contrasts at the soil–bedrock interface and digital elevation model-based physical flow path measurements to identify broad landscape trends of moisture redistribution in the subsurface of steep wet headwater catchments. We use this index to explore the relationship between geology, landscape structure, and water transit time through the lens of landscape anisotropy. We hypothesize that catchments with a greater tendency to shed water laterally will correlate with younger stream water MTT and catchments with a greater tendency to infiltrate water vertically will correlate with older stream water MTT. We tested the new index at eight geologically diverse Pacific Rim catchments in Oregon, Japan, and New Zealand. The new index explained 77% of the variability in measured stream water MTT across these varied sites. These findings suggest that critical zone anisotropy and catchment form are first-order controls on the time scales over which catchments store and release their water and that a simple index may usefully capture this relationship.

KEYWORDS

anisotropy, bedrock permeability, critical zone, headwaters, hydrology, landscape structure, mean transit time, turnover time

1 | INTRODUCTION

In its most basic form, the turnover time for water in a catchment follows the simple steady state equation $T = S/Q$, where T is the turnover time, S is the catchment storage, and Q is catchment discharge (Maloszewski & Zuber, 1982; McGuire & McDonnell, 2006; Staudinger et al., 2017). The time-varying nature of catchment conditions combined with the nonlinear and often hysteretic activation and deactivation of subsurface storage units and flow paths, however, results in a more complex and time-varying turnover time than this simple equation implies (Duffy, 2010; Heidbüchel, Troch, Lyon, & Weiler, 2012).

This complex storage–release interaction and catchment turnover time variation in space and time has been the subject of recent active theoretical research (Birkel, Soulsby, Tetzlaff, Dunn, & Spezia, 2012; Botter, Bertuzzo, & Rinaldo, 2011; Heidbüchel et al., 2012; Hrachowitz, Soulsby, Tetzlaff, Malcolm, & Schoups, 2010; Kirchner, 2016a; Kirchner, 2019). Contemporary particle tracking work (Ameli et al., 2017; Davies, Beven, Rodhe, Nyberg, & Bishop, 2013) and new complex storage selection functions (Harman, 2015; Rinaldo et al., 2015) have aimed to define the nonstationary nature of catchment discharge age across all catchment conditions.

But while much uncertainty still remains in terms of how fundamental critical zone (Grant & Dietrich, 2017) properties such as

geology, topography, vegetation cover, and seasonality in climate forcing control the time-varying age of water leaving a catchment (Hale & McDonnell, 2016; Heidbüchel, Troch, & Lyon, 2013; McNamara et al., 2011; Stewart, Morgenstern, Gusyev, & Małoszewski, 2017), few studies have explored the value of simple metrics in illuminating the control of subsurface architecture on catchment transit times. Here, we ask if there is a parallel, simple track perhaps worth exploring—a search for a basic catchment scale metric that might capture some of the overarching controls on catchment transit time—and in so doing convey insights into how critical zone form and subsurface structure influence internal catchment mixing dynamics that drive catchment storage–release processes. We base this on our recent work in geologically diverse catchments in Oregon, where McGuire et al. (2005) found landscape organization, specifically median flow path length divided by slope gradient, controlled catchment mean transit time (MTT)—defined as the average time water spends transiting the subsurface and stream channel before exiting the catchment outlet (McDonnell et al., 2010)—in seven nested catchments within the Oregon Cascade volcanics. Hale and McDonnell (2016) then tested this relationship in the Oregon Coast Range where more permeable meta-sedimentary bedrock showed no relation to topographic metrics but instead MTT was controlled by catchment area (where MTT increased as catchment area increased). These findings suggest that landscape-scale subsurface anisotropy (defined here as permeability contrast at the soil-bedrock interface) appears to be a first-order control on how catchments store and release their water. Hale et al. (2016) further expanded on the role of bedrock permeability in setting catchment scale storage–release patterns, identifying it as a critical catchment characteristic in controlling the age distribution of water exiting catchments in the Oregon Coast Range.

So how might this knowledge be incorporated into a simple index when so many model and theoretical approaches have been so complex? If we assume T as a proxy for MTT and start with the most basic form where MTT = S/Q, then decreases in S or increases in Q drive shorter MTT, and vice versa. Though this simplistic view is bedevilled by the complexity of interactions between inherent catchment properties, many field observations still come back to this ratio of storage and flux as a first approximation of MTT (Stewart, Mehlhorn, & Elliott, 2007). For example, catchment flux (i.e., Q) is directly controlled by precipitation or landscape gradient. Indeed, in different geologic and climatic settings, both Hrachowitz et al. (2009) and Heidbüchel et al. (2013) observed that increased annual precipitation led to shorter MTT, and in high relief landscapes, steep flow gradients are highly correlated with catchment transit times (Tetzlaff, Seibert, & Soulsby, 2009). Alternatively, differences in catchment storage (S), predominantly manifested as differences in soil thickness or bedrock permeability, have been found to control catchment MTT. Deeper more freely draining soils (Tetzlaff, Birkel, Dick, Geris, & Soulsby, 2014; Tetzlaff, Seibert, McGuire, Laudon, Burns et al., 2009) and greater percentages of more permeable bedrock (Pfister et al., 2017) both increase storage and result in longer catchment MTT.

Many efforts have been made with varying success to find simple scaling relationships between terrain-based indices and catchment transit times in order to shed light on the underlying storage–release relationship (Hale et al., 2016; Heidbüchel et al., 2013; McGlynn, McDonnell, Stewart, & Seibert, 2003; McGuire et al., 2005; McNamara et al., 2011; Soulsby, Piegat, Seibert, & Tetzlaff, 2011). Yet, most studies have lacked expansion of observation beyond their single study site or region, and none yet have found a simple terrain-based index that encapsulates both landscape form and geologic structure of the critical zone and their combined control on storage–release processes that can explain variations in the mean age of water discharged from different headwaters. Although Hale and McDonnell (2016) and Hale et al. (2016) came close, their work stopped short of any index development. Indeed, it has been observed for some time that strong subsurface permeability contrasts are key to initiation of lateral subsurface flow (Hopp & McDonnell, 2009), a flow mechanism that drastically shifts moisture redistribution from vertically downward—and thus through deeper more tortuous flow paths—to laterally and thus through shallow faster pathways: what Bonell (1993) called "throttles" for lateral flow.

Here, we present a new index to capture how critical zone anisotropy controls subsurface moisture redistribution and throttling. This work builds upon work by Hjerdt, Mcdonnell, Seibert, and Rodhe (2004) and Jackson, Bitew, and Du (2014), who developed the metric known as downslope travel distance (L_d). The Jackson et al. (2014) metric calculates the theoretical displacement of a parcel of water downslope before that parcel infiltrates into a lower impeding horizon. It was initially developed to calculate lateral travel distances in sequenced soil layers. Recently, Klaus and Jackson (2018) applied this index to 17 hillslopes across a range of landscapes and showed that in all but three cases, perched water tables infiltrated into the underlying impeding layer prior to reaching the stream channel. They used these findings to interpret hillslope–riparian–stream connectivity based on the presence of saturation across landscape. They found that a perched water table bridging landscape units does not make a hillslope–stream connection. Although the downslope travel distance calculation results in a theoretical distance, to date this distance has not been directly mapped to physical flow path lengths—in a single catchment or across catchments.

Here, we modify the Jackson downslope travel distance to focus specifically on the soil–bedrock interface as the impeding layer, and we integrate it with DEM-based physical flow path measurements to construct a new landscape scale anisotropy index (AI) that identifies broad scale landscape trends of moisture redistribution in the subsurface. We use this index to explore the relationship between geology, landscape structure, and water transit time through the lens of landscape anisotropy.

Specifically, we ask the following:

1. How do landscape form and critical zone anisotropy control subsurface flow partitioning and the tendency of a catchment to store or shed water?
2. Can an index that encapsulates this tendency towards shedding versus storage also capture observed variations in catchment stream water MTT?

We test this new index at eight well-studied headwater catchments in four geologically diverse regions within the Pacific Rim and compare differences in mean catchment index values with previously observed stream water MTT. We focus here initially on humid temperate catchments with thin soils and annual precipitation that greatly exceeds evapotranspiration and specifically where previous work has shown that despite similar rainfall–run-off characteristics, these catchments hide different geologically mediated subsurface run-off generation processes, thus providing an opportunity to highlight the role of subsurface architecture in differentially controlling catchment function (Hale & McDonnell, 2016; Katsuyama, Tani, & Nishimoto, 2010; McGuire et al., 2005; Sayama, McDonnell, Dhakal, & Sullivan, 2011).

2 | THEORY

Downslope travel distance is calculated as (1):

$$L_D = \frac{K_u}{K_L} * \frac{\sin\theta}{\frac{N+C_n}{C_n}} * N, \quad (1)$$

where K_u is the saturated hydraulic conductivity (K_{sat}) of overlying soil layer and K_L is the K_{sat} of the underlying impeding layer, here the bedrock horizon. N is the normal thicknesses of the saturated soil lens above the bedrock horizon, C_n is the thickness of saturated bedrock lens above the deeper regional water table, and θ is the local slope angle. This analysis assumes a pressure head of zero at the bottom of the saturated bedrock lens and assumed no connectivity between the perched water table and the regional aquifer below. For a more complete description, see Jackson et al. (2014).

We relate L_d to the physical landscape by dividing L_d by the flow path length (L_f) from the point of measurement on the landscape to the stream channel, to create the new AI. Figure 1 shows conceptually how the AI index functions. When AI is greater than 1, a parcel of water would require greater slope length to fully infiltrate into the underlying bedrock than is possible from the slope, and thus, the parcel of water is delivered to the stream channel. Conversely, when AI is less than 1, a parcel of water would move vertically through the soil and fully infiltrate into the bedrock horizon before reaching the stream channel, and thus, that parcel of water would be lost to deeper storage. Applying this calculation to each grid cell within a DEM provides a spatially distributed assessment of how a catchment internally redistributes its water. Taken in aggregate, the mean AI for a catchment provides information on the general tendency of the landscape to shed water laterally to the stream channel or infiltrate water to depth. We hypothesize that catchments with a lower mean AI and thus a greater proportion of water moving to depth through longer more tortuous flow paths will tend towards longer catchment MTT, and vice versa (Ameli, McDonnell, & Bishop, 2016; Jiang, Wan, Wang, Ge, & Liu, 2009).

3 | METHODS

We test this new index on eight well-studied watersheds in four geologically distinct regions around the Pacific Rim. Specifically, the M8 subcatchment within the Maimai Experimental Watershed, New Zealand (McGlynn, McDonnell, & Brammer, 2002), catchments WS1, WS9, and WS10 at the H.J. Andrews Experimental Forest Long Term Ecological Research site in the Cascade range of Oregon, USA (Swanson & Jones, 2002), catchments NB12, NB35, and NB86 recently studied by Hale and McDonnell (2016) and Hale et al. (2016)

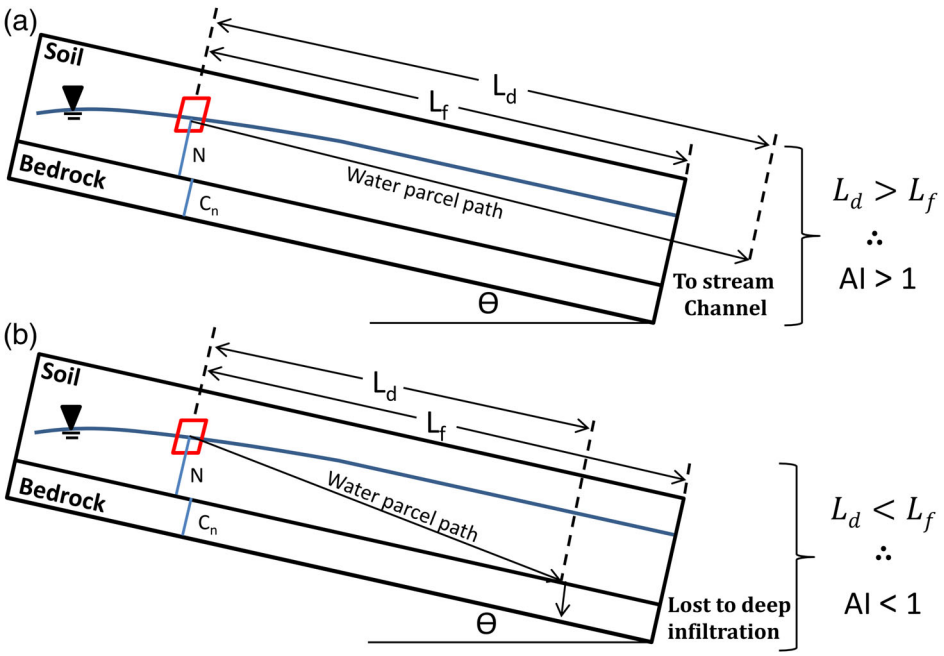

FIGURE 1 The modified Jackson index. When the anisotropy index (AI) is greater than 1, the downslope travel distance (L_d) of a parcel of water (here represented by the red box) is greater than the flow path length (L_f) that the parcel of water would travel down the hillslope to the stream channel. This results in the parcel of water being delivered to stream (a). When AI is less than 1, then L_d is greater than L_f and the parcel of water is lost instead to deep percolation. Figure adapted from Jackson et al. (2014)

within the coast range of Oregon, USA, and finally, catchment K at the Kiryu Experimental Watershed (KEW) in the Shiga Prefecture, Japan (Katsuyama, Fukushima, & Tokuchi, 2008). General catchment characteristics are presented in Table 1.

Catchments range in area from 4.5 (M8) to 86 ha (NB86); they have generally shallow soils (*M*: 0.9 m, *SD*: 0.19 m) and steep slopes (range: 1–65°, *M*: 30°, *SD*: 11°). Precipitation is high for all catchments, and with the exception of KEW, which receives on average 1,631 mm of rainfall, all catchments receive greater than 2,500 mm of rainfall annually. Previous work has established subsurface stormflow as the main run-off generating mechanism for all catchments.

Geologically, the catchments are quite diverse. M8 in New Zealand is underlain by an unfractured weakly cemented Early Pleistocene conglomerate composed primarily of sandstone clasts in a consolidated sandy matrix (Nathan, 1974). Bedrock at KEW is composed of a uniformly weathered Cretaceous biotite granite that is weathered in its upper layers to a saprolitic consistency (Katsura, Kosugi, Yamamoto, & Mizuyama, 2006; Torii, 1996). NB12, NB35, and NB86 in the Oregon Coast Range are composed of the Eocene-aged Tyee Formation, which are marine-derived layered greywacke siltstones and sandstones (Snavely, Wagner, & MacLeod, 1964), whereas bedrock in the Oregon Cascade Range catchments, WS1, WS9, and WS10, is composed of late Oligocene to early Miocene aged hydrothermally altered volcanic tuff and coarse breccia (Swanson & James, 1975).

Stream water MTT studies were conducted previously for all catchments, and we refer the reader to that primary literature as summarized in Table 2. The primary methodology employed to determine MTT was through lumped parameter convolution modelling using stable isotopes of water; however, tritium analysis combined with silica regression was used at M8 (Table 2). The authors recognize that MTT derived through time-invariant lumped convolution approaches can carry considerable uncertainty (Kirchner, 2016b) driving a shift away from MTT values as a descriptor of stream water transit time and towards time-varying transit time (Heidbüchel et al., 2012), storage-age functions (Harman, 2015), and percent young water (Kirchner, 2016a). However, this study is limited by the availability of data in the published literature, which in this case lacks values for the newer forms of stream water age computation for the tested watersheds.

MTT values ranged from 0.33 (M8) to 5.0 years (NB12). Previous work also investigated a range of catchment attributes that were observed to scale with or act as primary controls on catchment MTT (Table 2). This includes magnitude of annual bedrock infiltration (KEW; Katsuyama et al., 2010), catchment area (NB12, NB35, NB86; Hale & McDonnell, 2016), median subcatchment size (M8; McGlynn

TABLE 1 Summary of catchment characteristics

Catchment	Location	Area (ha)	Annual rainfall (mm)	Annual run-off (mm)	Run-off ratio, (—)	Mean soil depth, (m)	Elevation min (m a.s.l.)	Elevation max (m a.s.l.)	Geology
M8	Maimai Experimental Watershed, New Zealand	4.5	2600[a]	1550[a]	0.60	0.6[a]	250	348	Weakly cemented conglomerate[b]
WS1	HJ Andrews, LTER, OR, USA	96	2800[c]	1354[d]	0.48	0.9[d]	460	990	Volcanic tuff and coarse breccia[e]
WS9	HJ Andrews, LTER, OR, USA	8.5	2800[c]	1673[d]	0.60	0.9[d]	451	692	Volcanic tuff and coarse breccia[e]
WS10	HJ Andrews, LTER, OR, USA	10.2	2800[c]	1475[c]	0.53	3.0[f]	424	710	Volcanic tuff and coarse breccia[e]
KEW	Kiryu Experimental Watershed, Japan	5.99	1631[g]	936[h]	0.57	0.6[i]	178	253	Biotite granite[j]
NB12	Coast Range, OR, USA	12	2500[c]	1,627	0.65	1.0[c]	686	1,212	Marine-derived silt and sandstones[k]
NB35	Coast Range, OR, USA	35	2500[c]	1,588	0.64	1.0[c]	540	1,212	Marine-derived silt and sandstones[k]
NB86	Coast Range, OR, USA	86	2500[c]	1,548	0.62	1.0[c]	426	1,212	Marine-derived silt and sandstones[k]

[a]McGlynn et al. (2002).
[b]Pearce and Rowe (1979).
[c]Hale and McDonnell (2016).
[d]https://andrewsforest.oregonstate.edu/.
[e]Swanson and James (1975).
[f]Harr and Ranken (1972).
[g]Katsuyama et al. (2010).
[h]Katsuyama, Ohte, and Kobashi (2001).
[i]Kubota, Fukushima, and Suzuki (1983).
[j]Torii (1996).
[k]Snavely et al. (1964).

TABLE 2 Summary of catchment MTT characteristics

Catchment	MTT	MTT uncertainty	MTT determination method	MTT found to scale with…
M8	0.4[a]	± 0.1	Tritium and silica regression	[b]Median subcatchment area
WS1	1.3[c]	—	Stable isotopes of water and lumped-parameter convolution modelling	[c]Topographic characteristics, flow path length and gradient
WS9	0.8[c]	0.6/1.0 MTT ± 2σ	Stable isotopes of water and lumped-parameter convolution modelling	[c,d]Topographic characteristics, flow path length and gradient
WS10	1.2[c]	0.9/1.5 MTT ± 2σ	Stable isotopes of water and lumped-parameter convolution modelling	[c,d]Topographic characteristics, flow path length and gradient
KEW	4.1[e]	± 0.28	Stable isotopes of water and lumped-parameter convolution modelling	[e]Bedrock infiltration
NB12	5.0[c]	4.0/8.7 $MTT_{10/90\%}$	Stable isotopes of water and lumped-parameter convolution modelling	[c]Catchment area
NB35	3.7[c]	3.2/4.5 $MTT_{10/90\%}$	Stable isotopes of water and lumped-parameter convolution modelling	[c]Catchment area
NB86	4.0[c]	3.5/4.9 $MTT_{10/90\%}$	Stable isotopes of water and lumped-parameter convolution modelling	[c]Catchment area

[a]Gabrielli, Morgenstern, Stewart, and McDonnel (2018).
[b]McGlynn et al. (2003).
[c]Hale and McDonnell (2016).
[d]McGuire et al. (2005).
[e]Katsuyama et al. (2010).

TABLE 3 Catchment variables used to calculate the anisotropy index

Catchment	Soil K_{sat}, K_u (m/s)	Bedrock K_{sat}, K_L (m/s)	[a]Soil saturation depth: N, (m)	Bedrock saturation depth: Cn, (m)	Slope range, Θ, [°]	K_{sat} ratio, [–]
M8	6.94E–05[b]	9.90E–08[c]	0.3	1.0	2–51	702
WS1	1.00E–04[d]	1.42E–07[e]	0.5	1.0	1–69	706
WS9	1.00E–04[d]	1.42E–07[e]	0.5	1.0	4–45	706
WS10	1.00E–04[d]	1.42E–07[e]	1.5	1.0	1–45	706
KEW	4.70E–04[f]	1.00E–06[g]	0.3	1.0	1–41	470
NB12	2.78E–04[h]	4.70E–07[i]	0.5	1.0	1–44	591
NB35	2.78E–04[h]	4.70E–07[i]	0.5	1.0	1–44	591
NB86	2.78E–04[h]	4.70E–07[i]	0.5	1.0	1–46	591

[a]Depth of saturation was set equal to 0.5 times mean soil depth as reported in the listed literature in Table 2.
[b]McKie (1978).
[c]Gabrielli, Morgenstern, Steward and McDonell (2018).
[d]Ranken (1974).
[e]Graham, van Verseveld, Barnard and McDonnell (2010).
[f]Ohte, Suzuki, and Kubota (1989).
[g]Katsura et al. (2006).
[h]Hale and McDonnell (2016).
[i]Values based on nearby bedrock groundwater studies at the CB1 ridge (Montgomery, Dietrich, & Heffner, 2002) which were noted to have similar bedrock characteristics by Hale and McDonnell (2016).

et al., 2003), and flow path distance and gradient (WS9, WS10; McGuire et al., 2005).

Values for K_u and K_L in Equation (1) were established from catchment-specific literature as shown in Table 3. The thickness of the saturated lens above the impeding bedrock boundary, N, will vary both spatially and temporally and can take values ranging from 0 to the full thickness of the soil column. For simplicity, we used a spatially constant N equal to 0.5 times the mean catchment soil depth for all catchments, which corresponds well to piezometric observations at Maimai (McDonnell, 1990) and to observations made at similar catchments near both Oregon sites (Dhakal & Sullivan, 2014) for median-sized and larger storms. Similarly, the saturated bedrock thickness C_n can also vary spatially throughout a catchment and temporally under different catchment wetness

TABLE 4 Mean flow path length (L_f), mean downslope travel distance (L_d), mean AI, and percent $AI_{>1}$

Catchment	L_f mean (m)	L_f ± *SD* (m)	L_d mean (m)	±*SD* (m)	AI mean (–)	±*SD* (–)	Percent $AI_{>1}$, (%)
M8	25	22	98	15	8.0	6.8	1
WS1	121	34	122	76	3.8	6.3	34
WS9	119	22	126	76	3.8	6.4	35
WS10	100	49	228	64	6.9	11.5	8
KEW	26	12	38	16	3.3	2.7	18
NB12	254	12	32	151	0.6	0.8	92
NB35	256	12	54	195	0.6	0.6	92
NB86	287	12	56	214	0.5	0.6	93

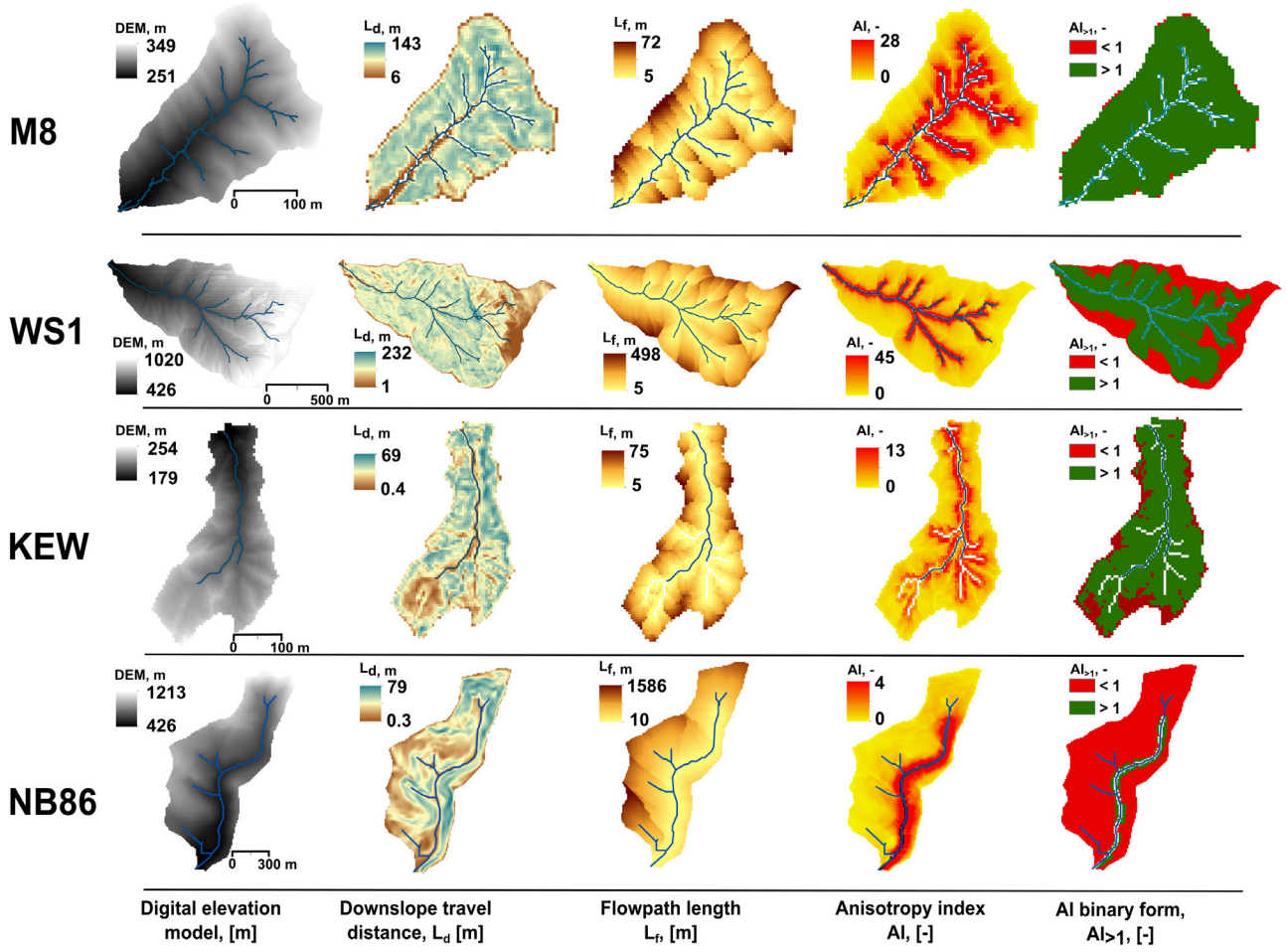

FIGURE 2 Catchment examples from the four different geologic settings. This figure shows, from left to right for each catchment, the sequence of analysis to calculate AI. The final graphic (far right) for each site shows the binary form of AI

conditions. Jackson et al. (2014) noted that C_n likely takes values ranging from very thin (<0.1 m) to very thick (>10 m). For simplicity, we used a spatially constant value of C_n equal to 1.0 m. However, we tested a range of values for both N and C_n and discuss the sensitivity of these variations to our final results in the discussion below. Local slope, Θ, was calculated for each catchment using a 5-m grid DEM, except for NB12, NB35, and NB86 in which a 10-m grid DEM was used.

L_f was calculated using the D8 flow algorithm (Jenson & Domingue, 1988) to determine flow path length from each grid cell to the stream channel. Stream channels were delineated based on stream initiation threshold values found in literature (Harris, 1977; Katsuyama et al., 2010; Pearce, Stewart, & Sklash, 1986; Rothacher, 1965). AI was calculated for each DEM grid establishing a spatially distributed AI map for each catchment. We calculated basic statistics for each catchment and compared mean AI to observed catchment MTT.

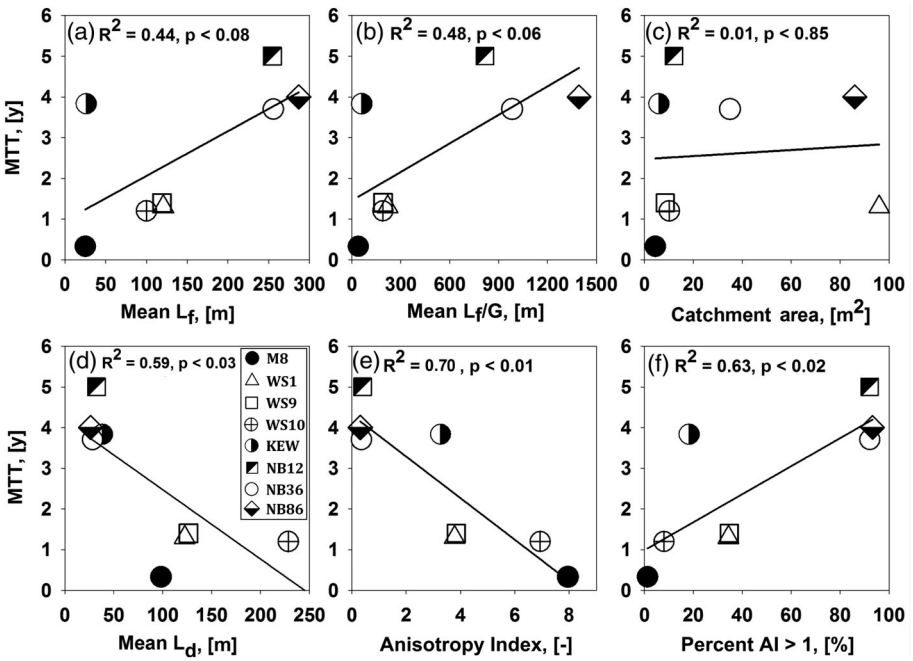

FIGURE 3 Relationship between the AI and catchment MTT for the eight studied catchments. The solid line shows the liner regression relationship between the two variables and the associated coefficient of determination. Note that catchment legend markers shown in (d) are consistent through all plots

4 | RESULTS

Table 4 presents mean values of L_f, L_d, and AI, as well as the percent coverage of AI values greater than 1 ($AI_{>1}$) for each of the eight study catchments. Mean catchment AI ranged from 0.3 at NB86 to 8.0 at M8. The three Oregon Coast Range catchments, NB12, NB36, and NB86, had the lowest mean AI as a result of a lower permeability contrast at the soil–bedrock interface and long hillslope lengths, which correspond with shorter downslope travels distances and longer flow path lengths. This suggests that water redistribution at these sites tends to be vertically downward into the bedrock horizon. Catchment M8 had the highest mean AI. The high soil–bedrock permeability contrast caused large downslope distances, yet physical slope lengths were short at M8, limiting total flow path length and increasing the tendency for the catchment to shed water laterally. Figure 2 shows the spatial distribution of each of these variables for four of the eight catchments—one each from the four geologic regions. Generally, catchments M8, WS1, and KEW had much higher AI in areas directly surrounding the stream channel. Values quickly dropped within distance upslope. Figure 2e shows the spatial distribution of $AI_{>1}$, distinguishing between grid cell values greater or less than 1. At M8, $AI_{>1}$ is present only in ridgeline locations, whereas at NB86, the inverse pattern was observed, and values were less than 1 across the majority of the catchment except directly along the stream channel. These two catchments provide bookend examples of landscape structures that tend to shed water (M8) versus infiltrate water (NB86).

We compared catchment MTT to catchment mean L_f, mean length/gradient (L_f/G), area, mean L_d, mean AI and $AI_{>1}$ (Figure 3). Both mean L_f and mean L_f/G explained about half of the variance observed in catchment MTT between the eight catchments (R^2 = .45 and .48, p < .01 and .02, respectively), whereas catchment area showed no correlation to MTT (R^2 = .01, p < .85). Mean L_d had a slightly stronger relation with MTT than L_f or L_f/G but still only explained slightly more than half of the variability observed in MTT. Mean AI, however, was strongly correlated to catchment MTT and explained nearly 80% of the observed variation in age (R^2 = .77, p < .01).

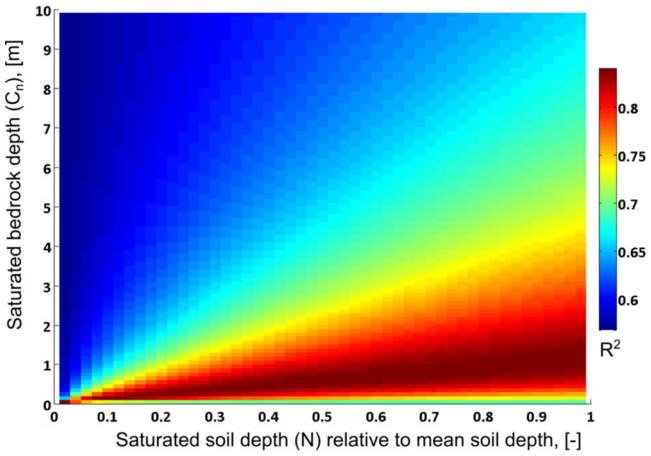

FIGURE 4 Coefficient of determination (R^2) values for the regression fit between catchment mean AI and MTT through a range of saturated soil depths (N) and saturated bedrock depths (C_n)

Since distributed field observations of soil and/or bedrock saturated thickness (N and C_n) are the most difficult data sets to obtain for this analysis and thus the most likely to contain large degrees of uncertainty due to estimation, we varied both N and C_n through a range of values and observed the sensitivity of the relationship between catchment mean AI and MTT through changes in the coefficient of determination (i.e., R^2). We varied N from 0.01 to 1 times the mean catchment soil depth and C_n from 0.1 to 10 m. Overall, the range in R^2 varied from .56 to .84, indicating the AI index still had a

strong relation with catchment MTT even if estimates of either parameter contained considerable uncertainty (Figure 4).

5 | DISCUSSION

5.1 | Critical contrasts in the critical zone

Although many studies have found landscape derived metrics at single sites that scale to MTT (Buttle, 2016; Hale & McDonnell, 2016; Katsuyama et al., 2010; McGlynn et al., 2003; McGuire et al., 2005; McNamara et al., 2011; Rodgers, Soulsby, Waldron, & Tetzlaff, 2005; Tetzlaff et al., 2009), we are unaware of any metric that successfully combines internal catchment structure with topographically based data to capture the observed variability in catchment discharge MTT across multiple geologically diverse sites. Our simple landscape AI builds on the Jackson et al. (2014) downslope travel distance index and combines simple field-measureable data with topographic DEM analysis into a single new composite index that captures the general tendencies of how catchments capture, store, and release their subsurface water. As the propensity to shed water laterally within a catchment increases (due to greater anisotropy at the soil–bedrock interface and/or shorter slopes lengths), greater relative volumes of water transit the subsurface domain through shallower faster flow paths, resulting in shorter MTT, and vice versa. Although stream water MTT is highly complex and varies considerably in time with catchment storage conditions (Harman, 2015; Heidbüchel et al., 2012; Maloszewski & Zuber, 1982; Morgenstern, Stewart, & Stenger, 2010; Tetzlaff et al., 2014), the general tendencies of subsurface storage and flow within a catchment are still reflected by their MTT values. Our results show a clear and significant relationship between mean AI and catchment MTT for eight catchments in four geological settings, highlighting the first-order control of subsurface anisotropy and catchment form on storage–release processes.

5.2 | On the meaning of AI

The AI index offers two levels of information: first through its spatially distributed pattern at the grid scale within each catchment and second through the catchment-scale mean value. At the grid scale, an individual grid value less than 1 indicates that a parcel of water originating from that grid cell will fully infiltrate into the underlying bedrock before reaching the stream channel. A grid-scale value greater than 1 indicates lateral movement of water to the stream and provides spatial information on variable source areas that contribute more extensively to the stream channel (Jackson et al., 2014; Walter et al., 2000). It is worth noting, however, that for grid values greater than 1, "transmission losses" to the bedrock horizon still occur as the parcel of water transits the hillslope. A grid value nearer to 1 implies greater transmission losses than a grid value further from 1, providing a means to compare the degree to which catchments move water to depth. This additional level of information is revealed by comparing the relationship of MTT with $AI_{>1}$ and mean AI (Figure 3e vs. 3f, respectively). The binary form of AI ($AI_{>1}$) does not account for transmission losses, which explains the weaker relationship. Mean AI captures this partial infiltration and more completely captures general catchment flux trends as indicated by the stronger correlation.

Although many catchments studied in this work showed clear MTT scaling relationships with different topographic or landscape-based metrics (Hale & McDonnell, 2016; McGlynn et al., 2003; McGuire et al., 2005), these metrics were not necessarily transferable between catchments in different geologic regions (Figure 3). This implies that local metrics such as area, slope gradient, and flow path distance do not always capture the full range of possible controls on MTT more generally. Our new AI captures between-region variability in MTT and provides strong evidence that it also captures the underlying relationships governing subsurface storage and release in these steep wet headwater catchments. This transcends single catchments finding and shows—at least for the environments tested here—that AI is able to subsume the previously identified dominant factors that mediate MTT at each individual catchment into a single value that captures broader controls on the relationship between geology, landscape structure, and catchment transit time.

So why does the AI outperform topographic metrics? In catchments with more than one major subsurface storage unit, bedrock permeability, and thus subsurface anisotropy, acts as a first-order control on the depth of active flow paths. In turn, the depth of active flow paths controls total mixing volume and the general flux rates of catchment storage, such that shallow flow paths tend to be faster and therefore younger (Hrachowitz et al., 2009; McGlynn et al., 2003), while deeper flow paths implicate larger storage and slower groundwater movement and tend to be older (Asano & Uchida, 2012; McNamara et al., 2011). AI identifies how MTT varies *between* catchments with different subsurface structures, whereas topographic metrics capture how MTT varies *within* catchments of generally similar geologic structure. In this manner, AI does not outperform topographic metrics, so much as it may be able to predict which metrics within a similar geologic unit scale with local catchment MTT. Catchments with similar geologic structure and a high AI would generally be associated with high permeability contrasts and shallow flow paths and thus young transits times, whereas the inverse would be true of catchments with low AI values.

5.3 | Beyond this very preliminary Pacific Rim testing

Although our index in no way replaces (nor do we argue against) ongoing work with particle tracking models (Ameli et al., 2017; Davies, Beven, Nyberg, & Rodhe, 2011) and storage selection functions (Kim et al., 2016; Klaus, Chun, McGuire, & McDonnell, 2015), this parallel learning track, with its simple approach, perhaps warrants further examination elsewhere. For ungauged catchments without MTT information, the AI index—with its ease of calculation and modest data requirements—offers an opportunity to explore how critical

zone structure and landscape form might shape the distribution of water ages discharged from catchments in various settings. This could be a useful hypothesis generating tool for field work and catchment modelling where such soft data exists (Sanford, 2002), especially in instances where theoretically, mathematically, and computationally intensive transit time models would be difficult to run.

Clearly, more testing needs to be done. The eight catchments tested in this study—although diverse geologically—are similar with respect to their high annual rainfall, high rainfall–run-off ratios, thin soils, and steep slopes. Groundwater recharge at these sites would be categorized as lithologically limited (Sanford, 2002); that is, deep infiltration is constrained by the ability of the subsurface to move water to depth, as opposed to being constrained by water availability. We need to test this index at drier sites and in locations where ET composes a greater proportion of the total water budget. We expect that climates with less precipitation or a higher evaporative index may be less likely to show similar trends with MTT, as the redistribution of moisture to depth would be controlled to a greater extent by factors other than geology. Additionally, for example, the well-known Scottish catchments of Rodgers et al. (2005) or Tetzlaff, Seibert, Mcguire, et al. (2009) and Ecuador sites of Mosquera et al. (2016) may reveal a different relation with the AI index due to peculiarities of soil drainage class, despite similar total rainfall patterns to the catchments tested here. Further, snowmelt-driven systems may perform well with this analysis as the steady drumbeat of daily meltwater shifts control moisture redistribution within the critical zone away from water availability to that of geologic and landscape structure.

Although we suspect this index may be limited to lithologically controlled groundwater systems, a larger analysis covering a wider array of catchment geologies, soil covers, and climates would be required to determine the full extent of these limitations and in so doing may shed light on alternative controls of MTT in different environments.

Lastly, although promising, our sensitivity analyses suggest that the index, although simple, may be partially limited by the availability of spatially robust soil and bedrock data sets and the ability to appropriately constrain effective catchment-scale hydraulic conductivity parameters. However, we showed strong correlations between catchment MTT and mean AI through a range of different C_n and N values, indicating a general lack of sensitivity to uncertainty in these values. This also suggests that the soil-to-bedrock permeability contrast is indeed the most critical component of the AI and its relation to catchment MTT in steep, headwater catchments—something that hillslope hydrological models have shown repeatedly for subsurface stormflow generation (Hopp & McDonnell, 2009; Jackson et al., 2016).

Further analyses may consider using spatially distributed soil thickness data where available. Additionally, where we used a spatially constant saturated soil thickness for this current analysis, it may be possible to incorporate a spatially distributed data set using proxy relationships between topographic indices, such as the topographic wetness index, and soil moisture (Sayama & McDonnell, 2009; Woods & Sivapalan, 1997) to construct a more precise spatially distributed catchment AI map. Further, this analysis may also be scaled to leverage recently established continental-scale permeability mapping (Gleeson et al., 2011) in an effort to predict large scale MTT trends that could provide a baseline for hypothesis testing to identify if landscapes follow or do not follow trends outlined by this index.

6 | SUMMARY

We show proof of concept for a new index that builds on recent work by Jackson et al. (2014) to quantify the relationship between geology, landscape structure, and water transit time within the critical zone. The AI successfully captures landscape scale water redistribution characteristics. We tested this relationship for eight catchments in four geologic settings and found a strong positive correlation between mean catchment AI and catchment stream water MTT that explained 70% of the variance in MTT. This suggests that permeability contrasts at the soil–bedrock interface in combination with hillslope flow path length act to control catchment scale storage characteristics that may account for the observed gross variability in catchment MTT.

ACKNOWLEDGEMENTS

The authors thank Ken Kosugi for the Kiryu Experimental Watershed DEM and Kevin McGuire and Cody Hale for their generous provision of data. Additionally, DEM data were provided by the HJ Andrews Experimental Forest and Long Term Ecological Research program, administered cooperatively by the US Department of Agriculture, Forest Service Pacific Northwest Research Station, Oregon State University, and the Willamette National Forest. This material is based upon work supported by the National Science Foundation under Grant DEB-1440409. The Oregon Geospatial Enterprise Office supplied the DEM data associated with the Needle Branch (NB) catchments. This work was supported through funding by NSERC Discovery grant to J.J. McDonnell and a Horton Research Grant to C.P. Gabrielli. Ali Ameli, Julian Klaus, Uwe Morgenstern, and Mike Stewart are thanked for early discussions on MTT. Lee Barbour, Andrew Ireson, Chris Spence, and Kelsey Jensco are thanked for early critical feedback on an earlier version of this paper. The late Mike Bonell is thanked for many early discussions on "throttles" for subsurface stormflow—something that he understood better than most. Finally, we thank our two reviewers for very insightful and helpful comments. The data that support the findings of this study are openly available at DOI 10.17605/OSF.IO/AH3WS.

DATA AVAILABILITY STATEMENT

The data that support the findings of this study are openly available at DOI 10.17605/OSF.IO/AH3WS In references: [dataset]Gabrielli, C P., McDonnell, J J. (2019); Anisotropy Index; OSF; DOI 10.17605/OSF.IO/AH3WS

ORCID

Christopher P. Gabrielli https://orcid.org/0000-0001-5085-5996

REFERENCES

Ameli, A., Mcdonnell, J., & Bishop, K. (2016). The exponential decline in saturated hydraulic conductivity with depth: A novel method for exploring its effect on water flow paths and transit time distribution. *Hydrological Processes*, *30*(14), 2438–2450. https://doi.org/10.1002/hyp.10777

Ameli, A. A., Beven, K., Erlandsson, M., Creed, I. F., Mcdonnell, J. J., & Bishop, K. (2017). Primary weathering rates, water transit times, and concentration-discharge relations: A theoretical analysis for the critical zone. *Water Resources Research*, *53*(1), 942–960. https://doi.org/10.1002/2016WR019448

Asano, Y & Uchida, T (2012). Flow path depth is the main controller of mean base flow transit times in a mountainous catchment. *Water Resources Research*, *48*(3), W03512. https://doi.org/10.1029/2011WR010906

Birkel, C., Soulsby, C., Tetzlaff, D., Dunn, S., & Spezia, L. (2012). High-frequency storm event isotope sampling reveals time-variant transit time distributions and influence of diurnal cycles. *Hydrological Processes*, *26*(2), 308–316. https://doi.org/10.1002/hyp.8210

Bonell, M. (1993). Progress in the understanding of runoff generation dynamics in forests. *Journal of Hydrology*, *150*, 217–275. https://doi.org/10.1016/0022-1694(93)90112-M

Botter, G., Bertuzzo, E., & Rinaldo, A. (2011). Catchment residence and travel time distributions: The master equation. *Geophysical Research Letters*, *38*(11), L11403. https://doi.org/10.1029/2011GL047666

Buttle, J. M. (2016). Dynamic storage: A potential metric of inter-basin differences in storage properties. *Hydrological Processes*, *30*(24), 4644–4653. https://doi.org/10.1002/hyp.10931

Davies, J., Beven, K., Nyberg, L., & Rodhe, A. (2011). A discrete particle representation of hillslope hydrology: Hypothesis testing in reproducing a tracer experiment at Gårdsjön, Sweden. *Hydrological Processes*, *25*(23), 3602–3612. https://doi.org/10.1002/hyp.8085

Davies, J., Beven, K., Rodhe, A., Nyberg, L., & Bishop, K. (2013). Integrated modeling of flow and residence times at the catchment scale with multiple interacting pathways. *Water Resources Research*, *49*(8), 4738–4750. https://doi.org/10.1002/wrcr.20377

Dhakal, A. S., & Sullivan, K. (2014). Shallow groundwater response to rainfall on a forested headwater catchment in northern coastal California: Implications of topography, rainfall, and throughfall intensities on peak pressure head generation. *Hydrological Processes*, *28*(3), 446–463. https://doi.org/10.1002/hyp.9542

Duffy, C. J. (2010). Dynamical modelling of concentration–age–discharge in watersheds. *Hydrological Processes*, *24*(12), 1711–1718. https://doi.org/10.1002/hyp.7691

Gabrielli, C. P., Morgenstern, U., Stewart, M. K., & McDonnell, J. J. (2018). Contrasting groundwater and streamflow ages at the Maimai watershed. *Water Resources Research*, *54*, 3937–3957. https://doi.org/10.1029/2017WR021825

Gleeson, T., Smith, L., Moosdorf, N., Hartmann, J., Dürr, H. H., Manning, A. H., & Jellinek, A. M. (2011). Mapping permeability over the surface of the Earth. *Geophysical Research Letters*, *38*(2), L02401. https://doi.org/10.1029/2010GL045565

Graham, C. B., van Verseveld, W., Barnard, H. R., & Mcdonnell, J. J. (2010). Estimating the deep seepage component of the hillslope and catchment water balance within a measurement uncertainty framework. *Hydrological Processes*, *24*(25), 3631–3647. https://doi.org/10.1002/hyp.7788

Grant, G. E., & Dietrich, W. E. (2017). The frontier beneath our feet. *Water Resources Research*, *53*(4), 2605–2609. https://doi.org/10.1002/2017WR020835

Hale, V. C., & Mcdonnell, J. J. (2016). Effect of bedrock permeability on stream base flow mean transit time scaling relations: 1. A multiscale catchment intercomparison. *Water Resources Research*, *52*(2), 1358–1374. https://doi.org/10.1002/2014WR016124

Hale, V. C., Mcdonnell, J. J., Stewart, M. K., Solomon, D. K., Doolitte, J., Ice, G. G., & Pack, R. T. (2016). Effect of bedrock permeability on stream base flow mean transit time scaling relationships: 2. Process study of storage and release. *Water Resources Research*, *52*(2), 1375–1397. https://doi.org/10.1002/2015WR017660

Harman, C. J. (2015). Time-variable transit time distributions and transport: Theory and application to storage-dependent transport of chloride in a watershed. *Water Resources Research*, *51*(1), 1–30. https://doi.org/10.1002/2014WR015707

Harr, R D & Ranken, D W (1972). Movement of water through forested soils in steep topography, p. 19, University of Washington, Coniferous Forest Biome Internal Rep. 117., Seattle, WA.

Harris, D. D. (1977). *Hydrologic changes after logging in two small Oregon coastal watersheds*. Geological Survey: Department of the Interior.

Heidbüchel, I., Troch, P. A., & Lyon, S. W. (2013). Separating physical and meteorological controls of variable transit times in zero-order catchments. *Water Resources Research*, *49*(11), 7644–7657. https://doi.org/10.1002/2012WR013149

Heidbüchel, I., Troch, P. A., Lyon, S. W., & Weiler, M. (2012). The master transit time distribution of variable flow systems. *Water Resources Research*, *48*(6), W06520. https://doi.org/10.1029/2011WR011293

Hjerdt, K. N., McDonnell, J. J., Seibert, J. & Rodhe, A. (2004). A new topographic index to quantify downslope controls on local drainage. *Water Resources Research*, *40*, W05602. https://doi.org/10.1029/2004WR003130

Hopp, L., & Mcdonnell, J. J. (2009). Connectivity at the hillslope scale: Identifying interactions between storm size, bedrock permeability, slope angle and soil depth. *Journal of Hydrology*, *376*(3–4), 378–391. https://doi.org/10.1016/j.jhydrol.2009.07.047

Hrachowitz, M., Soulsby, C., Tetzlaff, D., Dawson, J., Dunn, S., & Malcolm, I. (2009). Using long-term data sets to understand transit times in contrasting headwater catchments. *Journal of Hydrology*, *367*(3), 237–248. https://doi.org/10.1016/j.jhydrol.2009.01.001

Hrachowitz, M., Soulsby, C., Tetzlaff, D., Malcolm, I., & Schoups, G. (2010). Gamma distribution models for transit time estimation in catchments: Physical interpretation of parameters and implications for time-variant transit time assessment. *Water Resources Research*, *46*(10), W10536. https://doi.org/10.1029/2010WR009148

Jackson, C. R., Bitew, M., & Du, E. (2014). When interflow also percolates: Downslope travel distances and hillslope process zones. *Hydrological Processes*, *28*(7), 3195–3200. https://doi.org/10.1002/hyp.10158

Jackson, C. R., Du, E., Klaus, J., Griffiths, N. A., Bitew, M., & Mcdonnell, J. J. (2016). Interactions among hydraulic conductivity distributions, subsurface topography, and transport thresholds revealed by a multitracer hillslope irrigation experiment. *Water Resources Research*, *52*(8), 6186–6206. https://doi.org/10.1002/2015WR018364

Jenson, S. K., & Domingue, J. O. (1988). Extracting topographic structure from digital elevation data for geographic information system analysis. *Photogrammetric Engineering and Remote Sensing*, *54*(11), 1593–1600.

Jiang, X. W., Wan, L., Wang, X. S., Ge, S., & Liu, J. (2009). Effect of exponential decay in hydraulic conductivity with depth on regional groundwater flow. *Geophysical Research Letters*, *36*(24), L24402. https://doi.org/10.1029/2009GL041251

Katsura, S. Y., Kosugi, K. I., Yamamoto, N., & Mizuyama, T. (2006). Saturated and unsaturated hydraulic conductivities and water retention characteristics of weathered granitic bedrock. *Vadose Zone Journal*, *5*(1), 35–47. https://doi.org/10.2136/vzj2005.0040

Katsuyama, M., Fukushima, K., & Tokuchi, N. (2008). Comparison of rainfall-runoff characteristics in forested catchments underlain by granitic and sedimentary rock with various forest age. *Hydrological Research Letters*, *2*, 14–17. https://doi.org/10.3178/hrl.2.14

Katsuyama, M., Ohte, N., & Kobashi, S. (2001). A three-component end-member analysis of streamwater hydrochemistry in a small Japanese

forested headwater catchment. *Hydrological Processes*, *15*(2), 249–260. https://doi.org/10.1002/hyp.155

Katsuyama, M., Tani, M., & Nishimoto, S. (2010). Connection between streamwater mean residence time and bedrock groundwater recharge/discharge dynamics in weathered granite catchments. *Hydrological Processes*, *24*(16), 2287–2299. https://doi.org/10.1002/hyp.7741

Kim, M., Pangle, L. A., Cardoso, C., Lora, M., Volkmann, T. H., Wang, Y., & Troch, P. A. (2016). Transit time distributions and StorAge Selection functions in a sloping soil lysimeter with time-varying flow paths: Direct observation of internal and external transport variability. *Water Resources Research*, *52*(9), 7105–7129. https://doi.org/10.1002/2016WR018620

Kirchner, J. (2016a). Aggregation in environmental systems—Part 1: Seasonal tracer cycles quantify young water fractions, but not mean transit times, in spatially heterogeneous catchments. *Hydrology and Earth System Sciences*, *20*(1), 279–297.

Kirchner, J. W. (2016b). Aggregation in environmental systems—Part 2: Catchment mean transit times and young water fractions under hydrologic nonstationarity. *Hydrology and Earth System Sciences*, *20*(1), 299–328.

Kirchner, J. W. (2019). Quantifying new water fractions and transit time distributions using ensemble hydrograph separation: Theory and benchmark tests. *Hydrology & Earth System Sciences*, *23*(1), 303–349.

Klaus, J., Chun, K. P., Mcguire, K. J., & Mcdonnell, J. J. (2015). Temporal dynamics of catchment transit times from stable isotope data. *Water Resources Research*, *51*(6), 4208–4223. https://doi.org/10.1002/2014WR016247

Klaus, J., & Jackson, C. R. (2018). Interflow is not binary: A continuous shallow perched layer does not imply continuous connectivity. *Water Resources Research*, *54*(9), 5921–5932. https://doi.org/10.1029/2018WR022920

Kubota, J., Fukushima, Y., & Suzuki, M. (1983). Runoff characteristics and soil moisture variation of topsoil in head-waters of a mountain small catchment: The observation in weathered granitic mountains at the south-east of Shiga prefecture [Japan]. *Bulletin of the Kyoto University Forests (Japan) 55*, 162–181.

Maloszewski, P., & Zuber, A. (1982). Determining the turnover time of groundwater systems with the aid of environmental tracers. 1. Models and their applicability. *Journal of Hydrology*, *57*, 207–231. https://doi.org/10.1016/0022-1694(82)90147-0

McDonnell, J. J. (1990). A rationale for old water discharge through macropores in a steep, humid catchment. *Water Resources Research*, *26*(11), 2821–2832. https://doi.org/10.1029/WR026i011p02821

McDonnell, J. J., Mcguire, K., Aggarwal, P., Beven, K. J., Biondi, D., Destouni, G., & Kraft, P. (2010). How old is streamwater? Open questions in catchment transit time conceptualization, modelling and analysis. *Hydrological Processes*, *24*(12), 1745–1754.

McGlynn, B., Mcdonnell, J., Stewart, M., & Seibert, J. (2003). On the relationships between catchment scale and streamwater mean residence time. *Hydrological Processes*, *17*(1), 175–181. https://doi.org/10.1002/hyp.5085

McGlynn, B. L., Mcdonnell, J. J., & Brammer, D. D. (2002). A review of the evolving perceptual model of hillslope flowpaths at the Maimai catchments, New Zealand. *Journal of Hydrology*, *257*, 1–26. https://doi.org/10.1016/S0022-1694(01)00559-5

McGuire, K. J., & Mcdonnell, J. J. (2006). A review and evaluation of catchment transit time modeling. *Journal of Hydrology*, *330*(3), 543–563. https://doi.org/10.1016/j.jhydrol.2006.04.020

McGuire, K. J., Mcdonnell, J. J., Weiler, M., Kendall, C., Mcglynn, B. L., Welker, J. M., & Seibert, J. (2005). The role of topography on catchment-scale water residence time. *Water Resources Research*, *41*(5), W05002. https://doi.org/10.1029/2004WR003657

McKie, D (1978). A study of soil variability within the Blackball Hill soils, Reefton, New Zealand. Lincoln College, University of Canterbury.

McNamara, J. P., Tetzlaff, D., Bishop, K., Soulsby, C., Seyfried, M., Peters, N. E., & Hooper, R. (2011). Storage as a metric of catchment comparison. *Hydrological Processes*, *25*(21), 3364–3371. https://doi.org/10.1002/hyp.8113

Montgomery, D. R., Dietrich, W. E., & Heffner, J. T. (2002). Piezometric response in shallow bedrock at CB1: Implications for runoff generation and landsliding. *Water Resources Research*, *38*(12), 10-1–10-18. https://doi.org/10.1029/2002WR001429

Morgenstern, U., Stewart, M. K., & Stenger, R. (2010). Dating of streamwater using tritium in a post nuclear bomb pulse world: Continuous variation of mean transit time with streamflow. *Hydrology and Earth System Sciences*, *14*(11), 2289–2301. https://doi.org/10.5194/hess-14-2289-2010

Mosquera, G., Segura, C., Vaché, K., Windhorst, D., Breuer, L., & Crespo, P. (2016). Insights on the water mean transit time in a high-elevation tropical ecosystem 2. *Hydrology and Earth System Sciences*, *20*(1), 1–1, 3004. https://doi.org/10.5194/hess-20-2987-2016

Nathan, S. (1974). Stratigraphic nomenclature for the cretaceous-lower quaternary rocks of Buller and North Westland, west coast, South Island, New Zealand. *New Zealand Journal of Geology and Geophysics*, *17*(2), 423–445.

Ohte, N., Suzuki, M., & Kubota, J. (1989). Hydraulic properties of forest soils (I). *Journal of Japanese Forestry Society*, *71*(4), 137–147.

Pearce, A. J., & Rowe, L. K. (1979). Forest management effects on interception, evaporation. *And Water Yield. Journal of Hydrology*, *18*(2), 73–87.

Pearce, A. J., Stewart, M. K., & Sklash, M. G. (1986). Storm runoff generation in humid headwater catchments: 1. Where does the water come from? *Water Resources Research*, *22*, 1263–1272. https://doi.org/10.1029/WR022i008p01263

Pfister, L., Martínez-Carreras, N., Hissler, C., Klaus, J., Carrer, G. E., Stewart, M. K., & Mcdonnell, J. J. (2017). Bedrock geology controls on catchment storage, mixing and release: A comparative analysis of 16 nested catchments. *Hydrological Processes*, *31*(10), 1828–1845. https://doi.org/10.1002/hyp.11134

Ranken, D W (1974). Hydrologic properties of soil and subsoil on a steep, forested slope. M.S., Oregon State University, Corvallis.

Rinaldo, A., Benettin, P., Harman, C. J., Hrachowitz, M., Mcguire, K. J., van der Velde, Y., & Botter, G. (2015). Storage selection functions: A coherent framework for quantifying how catchments store and release water and solutes. *Water Resources Research*, *51*(6), 4840–4847. https://doi.org/10.1002/2015WR017273

Rodgers, P., Soulsby, C., Waldron, S & Tetzlaff, D (2005). Using stable isotope tracers to assess hydrological flow paths, residence times and landscape influences in a nested mesoscale catchment. *Hydrology and Earth System Sciences Discussions*, *9*(3), 139–155. hal-00304813

Rothacher, J. (1965). Streamflow from small watersheds on the western slope of the Cascade Range of Oregon. *Water Resources Research*, *1*(1), 125–134.

Sanford, W. (2002). Recharge and groundwater models: An overview. *Hydrogeology Journal*, *10*(1), 110–120. https://doi.org/10.1007/s10040-001-0173-5

Sayama, T., & Mcdonnell, J. J. (2009). A new time-space accounting scheme to predict stream water residence time and hydrograph source components at the watershed scale. *Water Resources Research*, *45*(7), W07401. https://doi.org/10.1029/2008WR007549

Sayama, T., Mcdonnell, J. J., Dhakal, A., & Sullivan, K. (2011). How much water can a watershed store? *Hydrological Processes*, *25*, 3899–3908. https://doi.org/10.1002/hyp.8288

Snavely, P. D., Wagner, H. C., & Macleod, N. S. (1964). Rhythmic-bedded eugeosynclinal deposits of the Tyee formation, Oregon Coast Range. *Kansas Geological Survey Bulletin*, *169*, 461–480.

Soulsby, C., Piegat, K., Seibert, J., & Tetzlaff, D. (2011). Catchment-scale estimates of flow path partitioning and water storage based on transit time and runoff modelling. *Hydrological Processes*, *25*(25), 3960–3976. https://doi.org/10.1002/hyp.8324

Staudinger, M., Stoelzle, M., Seeger, S., Seibert, J., Weiler, M., & Stahl, K. (2017). Catchment water storage variation with elevation. *Hydrological Processes*, *31*(11), 2000–2015. https://doi.org/10.1002/hyp.11158

Stewart, M. K., Mehlhorn, J., & Elliott, S. (2007). Hydrometric and natural tracer (oxygen-18, silica, tritium and sulphur hexafluoride) evidence for a dominant groundwater contribution to Pukemanga Stream, New Zealand. *Hydrological Processes*, *21*(24), 3340–3356. https://doi.org/10.1002/hyp.6557

Stewart, M. K., Morgenstern, U., Gusyev, M. A.., & Małoszewski, P. (2017). Aggregation effects on tritium-based mean transit times and young water fractions in spatially heterogeneous catchments and groundwater systems. *Hydrology and Earth System Sciences*, *21*(9), 4615–4627. https://doi.org/10.5194/hess-2016-532

Swanson, F J & James, M E (1975). Geology and geomorphology of the H.J. Andrews Experimental Forest, western Cascades, Oregon., p. 14, U.S. Department of Agriculture, Forest Service, Pacific Northwest Forest and Range Experiment Station, Portland, OR.

Swanson, F. J., & Jones, J. A. (2002). Geomorphology and hydrology of the HJ Andrews experimental forest, Blue River, Oregon. *Field Guide to Geologic Processes in Cascadia*, *36*, 289–313.

Tetzlaff, D., Birkel, C., Dick, J., Geris, J., & Soulsby, C. (2014). Storage dynamics in hydropedological units control hillslope connectivity, runoff generation, and the evolution of catchment transit time distributions. *Water Resources Research*, *50*(2), 969–985. https://doi.org/10.1002/2013WR014147

Tetzlaff, D., Seibert, J., Mcguire, K. J., Laudon, H., Burns, D. A., Dunn, S. M., & Soulsby, C. (2009). How does landscape structure influence catchment transit time across different geomorphic provinces? *Hydrological Processes*, *23*(6), 945–953. https://doi.org/10.1002/hyp.7240

Tetzlaff, D., Seibert, J., & Soulsby, C. (2009). Inter-catchment comparison to assess the influence of topography and soils on catchment transit times in a geomorphic province; the cairngorm mountains, Scotland. *Hydrological Processes*, *23*(13), 1874–1886. https://doi.org/10.1002/hyp.7318

Torii, A. (1996). Development of immature soils after afforestation on bare hills, with special reference to their mineralogical changes. *Journal of Forest Environment (Japan)*, *38*, 53–61.

Walter, M. T., Walter, M. F., Brooks, E. S., Steenhuis, T. S., Boll, J., & Weiler, K. (2000). Hydrologically sensitive areas: Variable source area hydrology implications for water quality risk assessment. *Journal of Soil and Water Conservation*, *55*(3), 277–284.

Woods, R. A., & Sivapalan, M. (1997). A connection between topographically driven runoff generation and channel network structure. *Water Resources Research*, *33*(12), 2939–2950. https://doi.org/10.1029/97WR01880

How to cite this article: Gabrielli CP, McDonnell JJ. Modifying the Jackson index to quantify the relationship between geology, landscape structure, and water transit time in steep wet headwaters. *Hydrological Processes*. 2020;1–12. https://doi.org/10.1002/hyp.13700